Geomorphology xxx (2012) xxx–xxx

Contents lists available at SciVerse ScienceDirect

Geomorphology

journal homepage: www.elsevier.com/locate/geomorph

PSInSAR displacements related to soil creep and rainfall intensities in the Alpine foreland of western Slovenia

Gorazd Žibret *, Marko Komac, Mateja Jemec

Geological Survey of Slovenia, Dimičeva ulica 14, SI-1001 Ljubljana, Slovenia

ARTICLE INFO

Article history:
Received 17 January 2011
Received in revised form 30 April 2012
Accepted 4 July 2012
Available online xxxx

Keywords:
Permanent scatterer
Soil creep
PSInSAR
Rainfall
Slovenia

ABSTRACT

An assessment of the relationship between displacement rates of objects located in areas of active soil creep and rainfall intensities was performed using a permanent-scatterer technique of synthetic aperture radar interferometry. The study focussed on two areas in central Slovenia during the period between April 1992 and December 2000. Based on field assessments, six permanent scatterers for one area and 11 scatterers for the other were selected for analysis from >4300 available permanent scatterers. Displacement rates related to creeping processes were compared with the different durations and intensities of rain in order to assess the threshold values that initiate the creeping process and to assess the relationship between the speed of the movement and the precipitation events. Although the permanent scatterer displacement data contain much noise, our results indicate that soil creep is induced by 20 mm of rain in 1 day or 50 mm of rain in 3 days, causing an average elevation decrease of 0.5 and 1 mm, respectively. The elevation decreases due to soil creep were observed as instantaneous events, since no increased correlations were observed when a time lag between precipitation and displacement was taken into account. Models developed in this research indicated very similar rates of tectonic uplift for the two research areas in the event of no rain, and these rates were found to be faster than the regional tectonic uplift. This suggests that areas with high rates of tectonic uplift and areas of active soil creep may be related.

1. Introduction

Gravitational slope mass movements in Slovenia constantly pose new challenges to experts who monitor and assess the dynamics and triggering mechanisms of such phenomena (Komac, 2006; Komac and Ribičič, 2006; Jemec and Komac, 2011). Among all possible forms of gravitational slope mass movements, soil creep poses several challenges to experts and civil engineers because such processes have spatially and temporally varying complex dynamics and can be very hard to detect. Experts are faced with the challenge of how to examine and study processes that are not only very slow and occur infrequently but are also monitored using processes other than the classical geotechnical methods. Another problem is that continuous monitoring over a wide area is difficult due to the lack of resources. This is why an approach that combines GIS, remote sensing, and data mining techniques must be applied in order to study soil creep processes.

Radar monitoring of the Earth's surface has improved dramatically in the past decade (Rott and Nagler, 2006; Bovenga et al., 2012). Numerous existing and planned satellites enable the continuous monitoring of almost every corner of our planet. Synthetic aperture radar (SAR) interferometry allows for the monitoring of surface displacements over wider areas (Fruneau et al., 1996; Berardino et al., 2002). The main advantages of SAR monitoring systems include their independence of solar illumination and cloud conditions as well as their relatively accurate measurements in the vertical (or subvertical) direction that range from several metres to less than a millimetre. Although more details of this method can be found in papers by Ferretti et al. (2001, 2005), Colesanti et al. (2003), and Oštir (2006), this approach is not ideal. The main problems with this method are related to the coherence, hidden sources of error in the radar signal (mainly due to atmospheric influence), and the temporal and spatial resolutions of the technique. Some of these obstacles can be overcome with the permanent scatterer interferometric technique (PSInSAR) (Oštir, 2000; Colesanti et al., 2003; Colesanti and Wasowski, 2006; Oštir and Komac, 2007). A permanent scatterer (PS; PSs is used for the plural form) is a natural outcrop or artificial object, such as a building, electrical power line, a metal structure with angular edges, or an artificial reflector. All PS displacements are relative to the reference point on the radar image that is considered stable in relation to the wider environs. The main constraints of the PSInSAR technique are the inability to detect displacements that occur (1) in vegetated areas, (2) in the North–south (N–S) direction, and (3) those larger than 28.3 mm (half of the wavelength of the radar signal; $\lambda = 56.6$ mm) between two image acquisitions, normally a period of 35 days. Further constraints include (4) the limited resolution of radar images (approximately 25 m), (5) rough terrain that causes shadowing effects and image distortion, and (6) the need for sufficient PS density, at least 4 km^{-2} (Colesanti et al., 2003). The quality of each PS is defined by a coherence value (γ),

* Corresponding author. Tel.: +386 1 2809 757; fax: +386 1 2809 753.
E-mail address: gorazd.zibret@geo-zs.si (G. Žibret).

0169-555X/$ – see front matter © 2012 Elsevier B.V. All rights reserved.
doi:10.1016/j.geomorph.2012.07.002

where a larger γ value means a better quality PS displacement time series (Colesanti and Wasowski, 2006; Oštir, 2006). Despite the aforementioned limitations, the PSInSAR technique can be successfully applied to the monitoring of slow processes (e.g. Carnec and Delacourt, 2000; Hilley et al., 2004; Salvi et al., 2004; Declerq et al., 2005; Bovenga et al., 2006; Farina et al., 2006). Therefore, the PSInSAR technique appears to be the most suitable for monitoring soil creeping processes.

Rainfall is recognised as an important factor that triggers the soil creep process in unstable or pseudo-stable slopes with thick layers of soil and weathered rocks, particularly in semi-humid and humid areas (Hinkelmann et al., 2011). However, there have not been many studies that relate gravitational mass movements to rainfall intensities. Studies focused on faster mass movement processes, mainly due to extreme weather events, use for visual correlations (event-response), while the PSInSAR technique has mostly been used for analysing slow-moving processes. Hilley et al. (2004) have detected the dependency of slowly-moving slope processes on rainfall and estimated that the lag of intensive movements could be up to 90 days. Ambrosi and Crosta (2006) detected a rise in PS displacement rates as a consequence of intensive rainfall in a period of over 1 year. Using PSInSAR measurements, Calabro et al. (2007) showed that this lag time varied from 14 to 42 days. Meisina et al. (2006) and Hu et al. (2009) found good visual correlation estimates of PS displacement rates with rainfall intensities. Iverson (2000) estimated that the lag time between the peak rainfall and landslide triggering moment varies from 5 to 8 days. On the other hand, Lollino et al. (2006) defined the lag time to be 8–9 days, while other studies (Guzzetti et al., 2004; Yu et al., 2006) reported shorter lag times that ranged up to 9 h during extreme weather events. According to Rotaru et al. (2007), creeping can also be related to either the pre-failure in (re)activation or the sliding retardation phase.

The main goal of this study is to assess the long- and short-term relationships between slow PS displacements, soil creep, and rainfall intensities in two areas in Slovenia where landslides and soil creep occur often. We also assessed the rainfall threshold amount that is needed to start the creeping process and the potential time lag between the rainfall event and the beginning of the creeping process. Satellite (PSInSAR), in-situ (visual estimation of the occurrence of soil creep), and precipitation data for the areas were combined through GIS to achieve the aforementioned goals.

2. Study area

Because rainfall is the main cause of gravitational slope mass movements, the northwestern part of Slovenia (Fig. 1) was chosen for this study due to its high annual precipitation rate (Zupančič, 1995). Combined with diverse lithostratigraphic and complex tectonic characteristics, this area is subjected to constant relief changes (Komac and Ribičič, 2006). These changes can be attributed to active tectonics (Poljak et al., 2000; Placer, 2008), the ongoing response to the ice retreat at the end of the Pleistocene (Bavec et al., 2004), and most significantly to the high annual average precipitation rates along with the related gravitational slope mass movements.

In general, the study area is exposed to moderate tectonic uplift, estimated to be between 1 mm year^{-1} (Komac and Bavec, 2007) and 5 mm year^{-1} (Rižnar et al., 2007). The study area extends from Stari Vrh (46°10′22.87″ N, 14°11′18.65″ E), which lies in the Alpine foreland

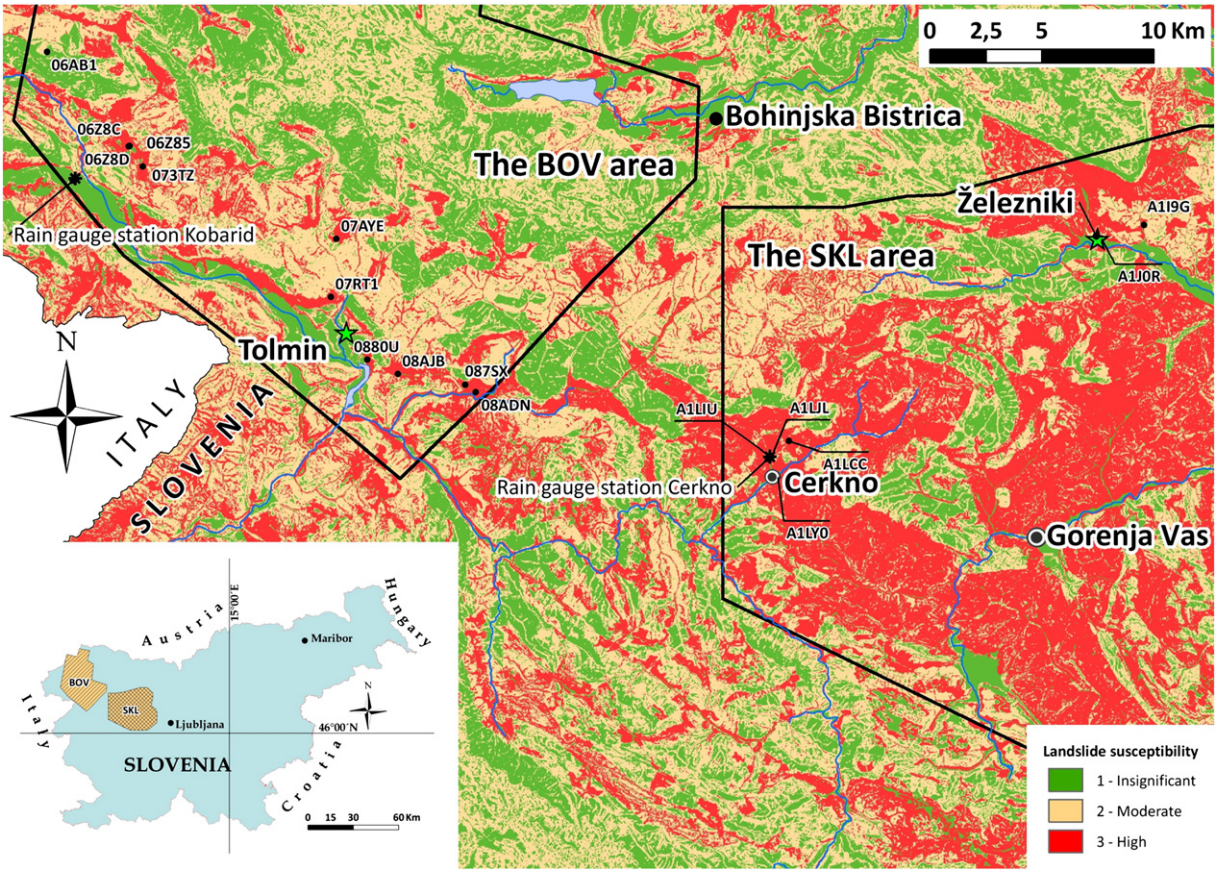

Fig. 1. Landslide susceptibility map (Komac and Ribičič, 2006) with the study areas (the BOV and the SKL areas), reference permanent scatterers (Tolmin for the BOV area and Železniki for the SKL area), locations of rain gauge stations (Kobarid and Cerkno), and locations of the permanent scatterers used (with names). The borders of the data acquisition campaign are outlined in a black line.

Please cite this article as: Žibret, G., et al., PSInSAR displacements related to soil creep and rainfall intensities in the Alpine foreland of western Slovenia, Geomorphology (2012), doi:10.1016/j.geomorph.2012.07.002

in the east, to Kobarid (46°14′48.36″ N, 13°35′5.47″ E), which lies in the Julian Alps in the west. The altitude ranges from 140 to 2660 m above sea level, and the mean slope angle is 24.1° with a standard deviation of 12.7°. Based on historical data, the area receives an annual average rainfall ranging from 1600 mm in the eastern section (Škofja Loka hills: the SKL area) to 3000 mm in the western section (Bovec: the BOV area) (Zupančič, 1995). The population of the area is approximately 80,000, with the majority of inhabitants concentrated in major towns such as Škofja Loka, Tolmin, Železniki, Cerkno, and Žiri. The geology of the study area is summarised in Buser (2010). The SKL area consists mainly of Mesozoic carbonates (limestones and dolomites), Mesozoic clastites (shales, siltstones, marlstones, grauwackes, sandstones, conglomerates, breccias, and tuffs), and Permian and Carboniferous clastites (claystones, sandstones, and shales). The valleys are mainly filled with alluvial deposits and the foot of slopes are typically covered by scree deposits, both of Quaternary age. The BOV area lies in the eastern flank of the Alpine chain and predominantly contains Mesozoic carbonates (limestones and dolomites), which, in some areas, change to less stable clastites such as marls, marlstones, and flysch. There are also numerous Quaternary scree deposits, i.e., rubble and remnants of past glacial activity such as tills and moraines. Based on GIS modelling, a landslide susceptibility map was made for this area (Komac and Ribičič, 2006) with three indices, from 1 (no possibility of landslides) to 3 (high risk of landslides) (Fig. 1).

3. Materials and methods

3.1. Raw data acquisition

For the interpretation of soil creep in relation to rainfall intensity, two datasets were acquired. The first dataset is the time-dependent PSInSAR measurement, which consists of two subsets, one for the western section (Alps) and the other for the eastern section (Alpine foreland) of the study area. All processed PSInSAR series were purchased from the Tele-Rilevemento Europa Company. Temporal availability was conditioned with the availability of the radar satellite data, although temporal separation between PS displacement measurements was in most cases 35 days. Despite the different intervals, all available measurements have been used in our research.

According to the Tele-Rilevemento Europa Company's report on InSAR data processing (TRE, 2008), the approach of averaging a number of images was used to minimise the random amplitude variability, leaving the uniform amplitude level unchanged. This technique is known as multi image reflectivity and is the means by which speckle reduction is accomplished. Atmospheric effects are eliminated or minimised with the first interferogram calculation, from which the atmospheric impact is estimated and removed based on the comparison to neighbouring pixels that are experiencing the same atmospheric conditions. Having removed the atmospheric artefacts, the data that remain are pixels (also referred to as PS candidates) that display stable amplitude and coherent phase throughout every image of the dataset. This correction is performed for each of the InSAR images. When these errors are removed, a history of radar signal phase values for each PS can be calculated and the shifts between the phases of different images can be derived. The phase shifts represent the displacements in the line-of-sight of the radar signal. The process is based on statistics and is accurate due to the large number of available images for the analysis.

The first PSInSAR dataset (the BOV area) covers 700 km^2 and consists of 1646 PSs with coherence values greater than 0.75. At each PS, the elevation change was measured 57 times (i.e., 57 InSAR images) in the period between 21 April 1992 and 29 December 2000 using the ERS-1 and ERS-2 data from the descending orbit. The time period between two consecutive measurements ranged from 35 to 583 days; this upper limit stems from the inactive period of the ERS satellites in 1994. On the other hand, some measurements were repeated in just 1 day (six cases); in such cases, the average value between the two measurements was used. The total number of measurements for the BOV dataset was thus 51 elevation change measurements for 1646 PSs. The image from 26 September 1997 was used as the master image (measurement). The total number of PSs was over 16,400, but only the best 10% met the temporal requirements and were used as input for the analysis. The average PS density for this subset was 23 PSs km^{-2}. The PS that is located in the town of Tolmin (46°11′3.44″ N, 13°44′45.12″ E) was defined as a reference point that acts as a stable object from which all PS displacements are calculated. The detected surface deformation in the study area ranged from −6.7 to 3.3 mm $year^{-1}$. In this paper, negative deformations or displacement rates denote elevation decreases or movement of the PS away from the satellite, whereas positive displacement rates denote elevation gains (uplift) or movement towards the satellite.

The second PS dataset (the SKL area) covers 643 km^2 and consists of 2786 PS measurements with coherence values greater than 0.58. Here, elevation change was measured during the period between 11 June 1992 and 10 December 2000. During this period, a total of 67 measurements (i.e., 67 InSAR images) from the descending orbit were acquired, with the time interval between measurements ranging from 35 to 548 days. When two measurements were made only 1 day apart, the same procedure as used for the BOV area was applied (i.e., the average value of two measurements). An image from 21 December 1997 was used as the master image. In this case, temporal displacement data were available for all 2786 PSs, and the average PS density for the subset was 4.33 PS km^{-2}. The PS located in the town of Železniki (46°13′32.05″ N, 14°10′31.77″ E) was defined as the reference point. Finally, the detected surface deformation in the study area ranged from −18.75 to 7.26 mm $year^{-1}$.

The precipitation dataset, acquired from the Environmental Agency of Slovenia, consists of daily rainfall measurements (in mm with a precision of 0.1 mm) between 1 January 1992 and 29 December 2000. This dataset covers the entire study area and includes 27 rain gauge stations. Fig. 2 shows an example of the raw precipitation data used in this study. The drawback of this data, which may slightly influence the results, is the unavailability of correctional information regarding snowmelt effects.

3.2. Field inspection of the PSs

Field inspection was carried out in order to determine the reasons for the PS elevation change, as well as to define the suitability of PSs for the analysis of precipitation influence on soil creep. This was necessary because there are factors other than soil creep and tectonics that govern PS elevation change. For instance, old abandoned wooden buildings, previously used for storing hay or crops, often have visible deterioration; when the roofs of these buildings act as PSs, the main reason for an elevation decrease is due to the decay of the wooden construction, not the tectonics or soil creep. One such example is presented in Fig. 3A. In total, 160 localities, containing approximately 500 PSs, were inspected, photographed, geologically evaluated, and described. Special attention was paid to visible signs of soil creep, such as tilted trees, characteristic land features, and cracks on buildings, among others. Further data processing was carried out for PSs that lay on solid foundations (Fig. 3B), such as roofs on concrete foundations, boulders, and roads on unstable terrain, where geologic conditions are favourable for slow gravitational slope processes (soil creep) and signs of such processes could be observed (e.g. tilted trees).

3.3. Data processing

Two main factors, excluding noise in the data and other non-geologically conditioned events, drive the elevation changes of the selected PSs: the first factor is tectonic activity that is potentially coupled with the uplift due to isostatic response from the latest ice retreat, and the second involves gravitational slope mass movements. In order to directly compare the PS vertical displacement rates with the aforementioned factors, which are expressed as a velocity (mm $year^{-1}$ or mm day^{-1}), the PS dataset was converted from absolute elevation values to elevation

Please cite this article as: Žibret, G., et al., PSInSAR displacements related to soil creep and rainfall intensities in the Alpine foreland of western Slovenia, Geomorphology (2012), doi:10.1016/j.geomorph.2012.07.002

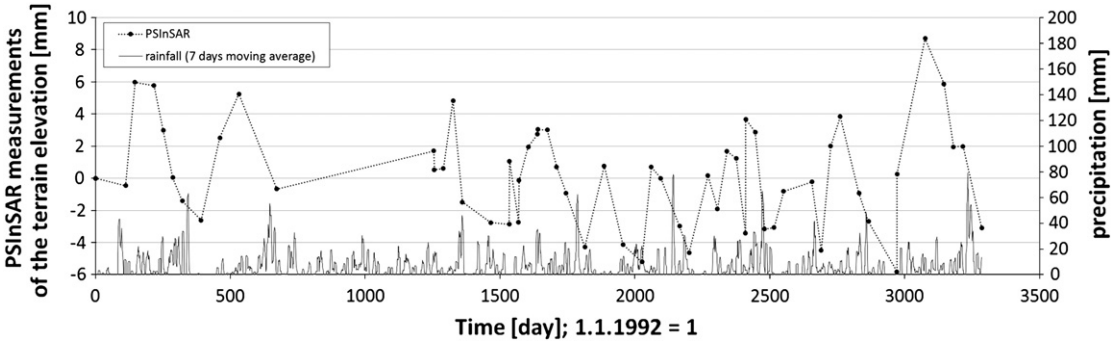

Fig. 2. Example of the raw datasets (07ZDO PSInSAR point and precipitation time series): time-dependent measurements of the terrain elevation and daily measurements of the rainfall nearby.

change rates (mm day^{-1}). The rates were calculated by dividing the observed differences in elevation between each pair of measurements by the number of days separating them.

The daily rainfall dataset was partitioned into precipitation parameters. These parameters were calculated by analogy of the PS displacement rates; rather than absolute values, they express occurrence rate or average precipitation for different time periods. This was necessary in order to directly determine the time-dependence of the elevation change on the intensity of the rainfall. All of the derived parameters were calculated for the time periods that exactly matched those of the PS displacement data acquisition. This means that the parameters were obtained by using the precipitation value (i.e., number of specific events or quantity of rain) and dividing this value by the time span of the observation in days. These parameters thus express the occurrence rate of a specific rainfall event (parameters with prefix "OR") or the average daily rainfall in a specific period (parameters with prefix "ADR"). The parameter name also has a second part that indicates the rain events of equal or greater intensity (in mm) that are taken into account. Thus, for example, the parameter ADR20 indicates the average daily rainfall (mm day^{-1}) where only rain events $\geq$20 mm are taken into account for a time period that exactly matches two consecutive PSInSAR data acquisitions. Descriptions of the nine derived parameters are given in Table 1.

Two sets of the derived rainfall parameters were used, where the first set was calculated using the raw data of the measured daily rainfall. However, such an approach is not sufficient enough for multi-day precipitation events. For example, the parameter ADR100 fails to detect a severe rainfall event where 90 mm of rain fell per day for three consecutive days (270 mm total). Thus, additional alterations to the dataset were required in order to include events where a large amount of rainfall occurred over a long time span. Intense precipitation in the study area normally lasts from several hours to several days (Vrhovec et al., 2004), and the monthly rainfall record for Slovenia was 1494 mm in November, 2000 (ARSO, 2010) at the weather station Soča (near a rain gauge that was used in our study). However, the dataset we used shows that high intensity rain events usually end after 2 days, as was the case with the November 2000 event. Because of this, we chose to base the rainfall data transformation on a three-day time period. The 20 mm precipitation threshold was used because the 20 mm daily rain events yielded the best correlations with the PS vertical displacement measurements (as shown in Section 4). The transformation was thus based on three conditions, where the sum of the rainfall during the three preceding days of the measurement was considered as one single rain event: 1) the amount of rainfall on the 3rd day must be the maximum in the 3 days, 2) on the day after (i.e., 4th day), there must be a decrease in rainfall, and 3) the sum of the cumulative rainfall over the 3 days must exceed 20 mm. If these conditions were not satisfied, we assumed there was no rain. Following such a transformation, the derived rainfall parameters were then calculated using the same procedure as above with the raw rainfall dataset, but are marked with asterisks (*) in order to distinguish them. Their names are as follows (6 parameters): OR20*, OR50*, OR100*, ADR20*, ADR50*, and ADR100*. Table 2 shows an example of the raw and transformed datasets, according to the described procedure, and Table 3 displays an example of the calculation used to obtain the parameters, utilising the dataset in Table 2. The next step involved calculating the correlation coefficients between the displacement rates and all 15 of the derived parameters, in order to see how well the PS displacement rates corresponded to the rainfall events. The Statistica application was used for this procedure. Regardless of the correlation value, each scatter plot was visually evaluated to avoid the misinterpretation of the obtained correlations.

Taking into account that rain generally requires some time to infiltrate the ground and initiate soil creep, we also tested the dataset for any possible lagged correlations between rainfall and the PS displacement rates using different time lags for rainfall (similar to a variogram, but a temporal one, not spatial). With this procedure, the potential temporal

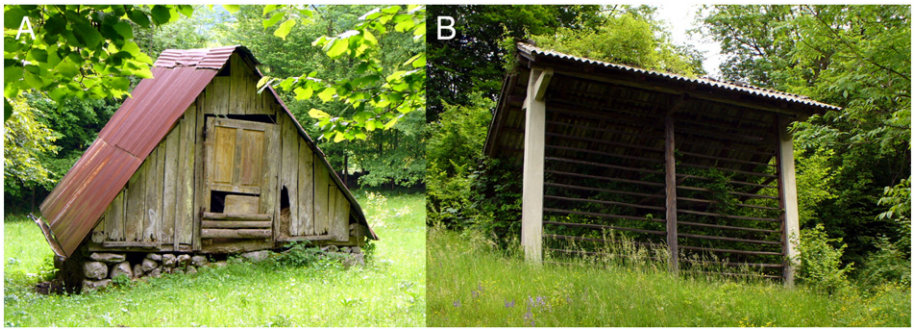

Fig. 3. Two examples of permanent scatterers. A) Example where the elevation change of −1.52 mm year^{-1} is most likely associated with the decay of the shed. Because of this, it was not used in our study, despite the fact that it is in an area of active soil creep. B) Solid concrete foundations in a soil creep area on Carboniferous and Permian shales and sandstones. Such PSs were used for further data processing.

Please cite this article as: Žibret, G., et al., PSInSAR displacements related to soil creep and rainfall intensities in the Alpine foreland of western Slovenia, Geomorphology (2012), doi:10.1016/j.geomorph.2012.07.002

Table 1
Description of the derived rainfall parameters. p_i: a sequence of daily precipitation measurements expressed as mm day^{-1}. $t \rightarrow t+\Delta t$: time periods between two consecutive measurements of permanent scatterer vertical displacement; t is a natural number and denotes days with 1.1.1992 to be a day 1; $t \in N$; $1 \leq t \leq t_{max}$; $t_{max} = 3267$. $|\{A\}|$: cardinality of the set A (the number of the elements in the set A). $\wedge$: logical "and".

Parameter name	Parameter definition	Description
OR5	$=\lvert\{p_i: p_i>5 \text{ mm} \wedge i=t, t+1,\ldots, t+\Delta t\}\rvert\Delta t^{-1}$	Occurrence rate of >5 mm rain events
OR20	$=\lvert\{p_i: p_i>20 \text{ mm} \wedge i=t, t+1,\ldots, t+\Delta t\}\rvert\Delta t^{-1}$	Occurrence rate of >20 mm rain events
OR50	$=\lvert\{p_i: p_i>50 \text{ mm} \wedge i=t, t+1,\ldots, t+\Delta t\}\rvert\Delta t^{-1}$	Occurrence rate of >50 mm rain events
OR100	$=\lvert\{p_i: p_i>100 \text{ mm} \wedge i=t, t+1,\ldots, t+\Delta t\}\rvert\Delta t^{-1}$	Occurrence rate of >100 mm rain events
ADR	$=\Sigma(p_i: i=t, t+1,\ldots, t+\Delta t)\Delta t^{-1}$	Average daily rainfall
ADR5	$=\Sigma(p_i: p_i>5 \text{ mm} \wedge i=t, t+1,\ldots, t+\Delta t)\Delta t^{-1}$	Average daily rainfall, only >5 mm events
ADR20	$=\Sigma(p_i : p_i>20 \text{ mm} \wedge i=t, t+1,\ldots, t+\Delta t)\Delta t^{-1}$	Average daily rainfall, only >20 mm events
ADR50	$=\Sigma(p_i: p_i>50 \text{ mm} \wedge i=t, t+1,\ldots, t+\Delta t)\Delta t^{-1}$	Average daily rainfall, only >50 mm events
ADR100	$=\Sigma(p_i: p_i>100 \text{ mm} \wedge i=t, t+1,\ldots, t+\Delta t)\Delta t^{-1}$	Average daily rainfall, only >100 mm events

difference between the rainfall event and the actual gravitational slope mass movement was assessed. The time lags used were 0, 3, 7, 14, 30, 60, and 90 days.

The correlation coefficients between soil creep (expressed as PS displacements rates) and rainfall were calculated separately for each area due to the different reference points for the two study areas. Moreover, the correlations and other types of data processing used separate rainfall data for each area. For the BOV area, rainfall data from the rain gauge station Kobarid were used, and for the SKL area, the data from the rain gauge station Cerkno were used. Therefore, the datasets were not comparable with each other and had to be treated separately.

4. Results and discussion

After the in-situ inspection, 11 PSs in the BOV area and 6 PSs in the SKL area were selected for further analysis. This large reduction of the dataset, from a total of 4432 PSs to the final 17, had to be done in order to ensure that only the most suitable PSs were used for further analysis. The criteria that defined the final selection of PSs were a high enough coherence value (>0.58), a solid construction (Fig. 3), and a placement on an area of active soil creep. Table 4 shows the correlation coefficients between the displacement rates and the derived precipitation parameters. Fig. 4 shows an example of the scaling of the displacement rates of the PS 0880U (shown in Fig. 1) with the occurrence rate of the rainfall event (parameter OR20*).

For the evaluation of which rainfall parameter (and the precipitation level that is derived from it) best corresponds to the soil creep process, the average correlation coefficients of the suitable PSs for the BOV and SKL areas were calculated (Table 4). A higher absolute correlation coefficient suggests a stronger dependency. The results suggest that lower intensity precipitation events (between 5 and 50 mm in 1 day) also contribute to soil creep; this was surprising as it was primarily expected that only strong rain events would have this effect. This also applied to situations where the same small rate of precipitation occurred over a longer period (3 days in our case; parameters with *).

Furthermore, linear models of soil creep rate in relation to the probability of rain events were made. Only the parameters that deal with the number of rain events can be used for this purpose. To derive such models, the PS displacements rates and precipitation parameters that expressed the highest average correlation and the highest number of significant correlations (Table 4) were used for both 1-day and 3-day events. The parameters that meet these conditions are OR20 (Fig. 5A) and OR50* (Fig. 5B) for the BOV area, and OR20 (Fig. 5C) and OR20* (Fig. 5D) for the SKL area. Two points on the obtained regression line are important and require further discussion. The first point is the value of vertical displacement when there is a zero occurrence rate for rain events; this value indicates the average tectonic uplift for the PSs (and their environs). The second point is obtained when the occurrence rate of the rain event is equal to 1. If one subtracts the tectonic uplift from this second value, the resulting number is equivalent to the average vertical change due to soil creep, as a consequence of a precipitation event.

In the BOV area, the tectonic uplift is estimated to be between 0.035 (Fig. 5A) and 0.042 (Fig. 5B) mm day^{-1}. This corresponds to an annual tectonic uplift of 13–15 mm year^{-1}. For the SKL area, these values are slightly greater, between 0.051 (Fig. 5C) and 0.077 (Fig. 5D) mm day^{-1}, or 19–28 mm year^{-1}. The regional tectonic uplift for the region is estimated to be 14 mm year^{-1} (Komac and Bavec, 2007; Rižnar et al., 2007), but this value is subject to different local deviations due to the complex tectonic and geological structure of the area (Kastelic et al., 2008; Lajmiš et al., 2011). It must also be taken into account that the values obtained in this study do not show absolute displacements, but rather displacements relative to a reference point, which is also subject to regional tectonic activity. This means that the tectonic uplift in areas of active soil creep is larger than the regional tectonic uplift by 13–28 mm year^{-1}. Such a result might indicate that soil creep is associated with areas of higher tectonic uplift than the regional average, if geological and other conditions are favourable for soil creep. This is likely to be the case as both areas are dissected by faults, making the region highly tectonically heterogenic.

As mentioned before, the second significant point on the regression lines indicates the magnitude of the vertical displacement due to soil creep, which is a consequence of a rain event. In the case of an average ≥20 mm precipitation event (in 1 day), the surface is displaced away from the satellite by −0.4 mm in the BOV area and by −0.76 mm in the SKL area. The obtained vertical displacement of the terrain away from the satellite for an average three-day ≥50 mm precipitation event is −0.87 mm for the BOV area. The displacement for an average three-day ≥20 mm rain event is −1.2 mm for the SKL area. The differences in the average vertical displacements with regard to the precipitation events for both areas can be attributed to the different geological settings where the PSs are situated. In general, the terrain in the SKL area is more susceptible to landslide occurrence (average landslide susceptibility of 2.7 out of 3) than the terrain in the BOV area (susceptibility of 1.9) (Table 4). Thus, it is expected that displacements of the PSs in the SKL area can be triggered by lower precipitation intensities than the BOV area.

Table 2
Example of the transformation for the rain events.

Day	t	t+1	t+2	t+3	t+4	t+5	t+6	t+7	t+8	t+9	t+10	t+11	t+12	t+13	t+14	t+15	t+16	t+17	t+18	t+19
Raw [mm]	3.5	26.1	44.7	13.9	26.9	10.6	18.4	13.0	72.1	14.3	0.0	0.0	0.0	0.0	0.0	3.6	32.7	104.9	27.4	0.7
Transformed	0.0	0.0	74.3	0.0	0.0	0.0	0.0	0.0	103.5	0.0	0.0	0.0	0.0	0.0	0.0	0.0	0.0	141.2	0.0	0.0

Please cite this article as: Žibret, G., et al., PSInSAR displacements related to soil creep and rainfall intensities in the Alpine foreland of western Slovenia, Geomorphology (2012), doi:10.1016/j.geomorph.2012.07.002

Table 3
Calculation of the precipitation variables using data from Table 2.

Parameter	OR5	0R20	OR50	OR100	ADR	ADR5	ADR20	ADR50	ADR100
Value [mm day^{-1}]	0.632	0.368	0.105	0.0526	21.7	21.3	17.6	9.32	5.52
Parameter	–	0R20*	OR50*	OR100*	–	ADR5*	ADR20*	ADR50*	ADR100*
Value [mm day^{-1}]	–	0.158	0.158	0.105	–	16.8	16.8	16.8	12.9

The results of the temporal dependence test of the gravitational slope mass movements on rainfall intensities are presented in Fig. 6. This test was made only with the occurrence rate precipitation parameters that had the highest correlations with the negative displacement rates. These parameters are OR20 and OR50* for the BOV area and OR20 and OR20* for the SKL area. As the time lag between the actual precipitation event and the mass movement measurement increases, the correlations drop significantly. No significant correlations are recorded for a lag of 30 days or more. This result implies that rainfall induces instant mass movements. The trend of increased correlation coefficient values at a lag of 90 days, especially for the SKL area, should be regarded as an artefact, because coincidently, some heavy precipitation events occur approximately 90 days apart, such as the events on 12 July and 7 October 1993 (88 days), 23 June and 20 September 1995 (90 days), and 3 July and 3 October 1996 (93 days).

The average correlation values for both areas (Table 4) indicate the precipitation events that trigger the most soil creep. The highest correlations for the BOV area are found for the parameters OR20, ADR, ADR5, OR20*, OR50*, and ADR20*. Heavy precipitation parameters, such as OR100 and ADR100, show significantly lower correlations. Similar results are also detected for the SKL area, where the highest correlations are found for the precipitation parameters OR20, ADR20, OR20*, and ADR20*. This means that soil creep is caused not only by heavy rain events but also by lower intensity events. Our results indicate that the negative elevation change of PSs are best correlated to the rain events of ≥20 mm, and it does not matter significantly whether such events occur over 1 or 3 days.

Overall, it should be considered that there are disadvantages and limitations of using PSInSAR data for this type of research, which results in poor correlations (the largest correlation is −0.48 for the vertical displacement rate of PS 0880U with the OR20* precipitation parameter). This suggests that individual rainfall events have a greater influence or the response window or lag time is very short, something which is not detected with the PSInSAR methodology since PS vertical displacement measurements take place every 35 days or more. The methodology used in our research was also not able to detect soil creep during very intense rain events. The poor correlation between PS displacement rates and extreme rainfall events (≥100 mm day^{-1}) can be attributed firstly to the small and unrepresentative number of such events. In the SKL area, there were only three events with precipitation over 100 mm day^{-1}, while in the BOV area, there were eight such events. The second reason for the poor correlation could be the fact that heavy rainfall triggers other, faster types of slope mass movements resulting in displacements of a higher order of magnitude, which cannot be detected by the PSInSAR technique. As previously mentioned, the displacement detection limit of the PSInSAR technique is 0.8 mm day^{-1} or 28 mm in 35 days. In addition, snow cover can induce soil creep in both research areas but was not taken into account in this study. The data regarding the height of the snow cower was missing, thus the contribution of snowmelt to the quantity of ground water was not considered. This effect certainly adds some additional noise in the dataset, but we think it not enough to change our main results.

5. Conclusions

The relationship between daily rainfall and displacement rates of objects located on areas of active soil creep, as measured by the PSInSAR technique, was addressed in this study. Data of displacement rates for 11 PSs in the BOV area and 6 PSs in the SKL area as well as daily rainfall data throughout an eight-year period was used for this purpose. Our results indicate that soil creep can be triggered by low-intensity rainfall. The greatest influence on PS displacement rates was detected with rainfall intensities of ≥20 mm in 1 day or an accumulation of ≥20 mm over 3 days. Rain events of lower intensities were not found to be an important factor for triggering soil creep process. Developed models showed that a rainfall event of ≥20 mm day^{-1} results in an elevation change

Table 4
Correlation coefficients between the displacement rates and rainfall parameters. Bold numbers represent statistically significant correlations for the significance level of 95%. LS: landslide susceptibility model value (Komac and Ribičič, 2006). C: coherence. Vel: average 10-year displacement rate [mm year^{-1}]. AVG: average values.

Code	LS	C	Vel	OR5	OR20	OR50	OR100	ADR	ADR5	ADR20	ADR50	ADR100	OR20*	OR50*	OR100*	ADR20*	ADR50*	ADR100*
The BOV area																		
06AB1	1	0.75	2.07	**−0.37**	−0.25	−0.18	−0.12	**−0.31**	**−0.30**	−0.25	−0.19	−0.16	**−0.30**	−0.28	−0.15	−0.27	−0.25	−0.16
06Z85	0	0.77	−1.20	**−0.29**	−0.27	−0.28	−0.18	**−0.30**	**−0.30**	**−0.28**	−0.27	−0.20	**−0.37**	**−0.37**	−0.27	**−0.34**	**−0.32**	−0.26
06Z8C	0	0.79	−0.26	**−0.40**	**−0.32**	**−0.35**	**−0.36**	**−0.38**	**−0.38**	**−0.34**	**−0.33**	**−0.32**	**−0.30**	**−0.36**	**−0.28**	**−0.35**	**−0.33**	−0.27
06Z8D	0	0.85	−0.87	**−0.39**	**−0.45**	**−0.31**	−0.22	**−0.36**	**−0.36**	**−0.34**	−0.26	−0.16	**−0.46**	**−0.33**	−0.28	**−0.38**	**−0.30**	−0.24
073TZ	3	0.85	−1.23	−0.22	**−0.35**	−0.27	−0.23	**−0.35**	**−0.35**	**−0.37**	**−0.32**	−0.28	−0.24	**−0.41**	−0.27	**−0.33**	**−0.36**	−0.27
07AYE	3	0.76	−1.02	−0.11	−0.21	**−0.34**	−0.28	−0.24	−0.24	−0.28	**−0.34**	−0.25	−0.28	**−0.28**	−0.25	**−0.34**	**−0.32**	−0.27
07RT1	3	0.75	−1.34	**−0.30**	**−0.34**	−0.02	0.01	−0.23	−0.23	−0.20	−0.07	−0.06	**−0.33**	**−0.38**	−0.05	−0.25	−0.24	−0.06
087SX	3	0.74	−0.96	−0.13	**−0.34**	−0.16	−0.22	**−0.28**	**−0.29**	**−0.33**	−0.26	−0.26	−0.26	**−0.34**	−0.27	**−0.34**	**−0.34**	−0.27
0880U	2	0.75	−1.09	**−0.37**	**−0.37**	−0.16	−0.26	**−0.37**	**−0.36**	**−0.34**	−0.22	**−0.30**	**−0.48**	−0.21	−0.25	**−0.36**	−0.25	−0.24
08ADN	3	0.74	−2.06	**−0.36**	−0.24	−0.25	**−0.28**	**−0.33**	**−0.33**	**−0.29**	**−0.28**	**−0.30**	−0.23	−0.26	**−0.31**	**−0.34**	**−0.33**	**−0.34**
08AJB	3	0.75	−0.99	**−0.44**	**−0.37**	**−0.36**	−0.26	**−0.37**	**−0.38**	**−0.33**	**−0.30**	−0.21	**−0.30**	**−0.34**	−0.25	**−0.35**	**−0.33**	−0.25
AVG	1.9			−0.31	−0.32	−0.24	−0.22	−0.32	−0.32	−0.30	−0.26	−0.23	−0.32	−0.32	−0.24	−0.33	−0.31	−0.24
The SKL area																		
A1LYO	2	0.83	−4.37	**−0.33**	−0.22	−0.16	−0.14	**−0.32**	**−0.32**	**−0.29**	−0.19	−0.14	−0.16	**−0.32**	**−0.42**	**−0.28**	**−0.34**	**−0.40**
A1I9G	2	0.85	0.03	**−0.28**	**−0.31**	−0.13	−0.10	**−0.28**	**−0.28**	**−0.27**	−0.13	−0.10	**−0.38**	−0.25	−0.12	**−0.33**	−0.24	−0.12
A1J0R	3	0.61	−0.72	**−0.33**	**−0.38**	**−0.32**	−0.06	**−0.36**	**−0.36**	**−0.36**	**−0.30**	−0.06	**−0.36**	**−0.32**	−0.11	**−0.34**	**−0.30**	−0.09
A1LCC	3	0.71	1.52	−0.26	**−0.32**	**−0.30**	−0.12	**−0.28**	**−0.28**	**−0.28**	**−0.28**	−0.12	**−0.37**	−0.12	0.12	**−0.28**	−0.13	0.11
A1LIU	3	0.63	1.01	−0.14	**−0.35**	−0.21	−0.11	−0.26	−0.26	**−0.32**	−0.22	−0.11	**−0.35**	−0.13	0.00	**−0.30**	−0.14	0.00
A1LJL	3	0.58	−0.12	−0.18	**−0.32**	−0.22	−0.08	−0.23	−0.24	**−0.29**	−0.22	−0.08	**−0.27**	**−0.27**	−0.16	**−0.28**	**−0.27**	−0.15
AVG	2.7			−0.25	−0.32	−0.22	−0.10	−0.29	−0.29	−0.30	−0.22	−0.10	−0.32	−0.23	−0.11	−0.30	−0.24	−0.11

Please cite this article as: Žibret, G., et al., PSInSAR displacements related to soil creep and rainfall intensities in the Alpine foreland of western Slovenia, Geomorphology (2012), doi:10.1016/j.geomorph.2012.07.002

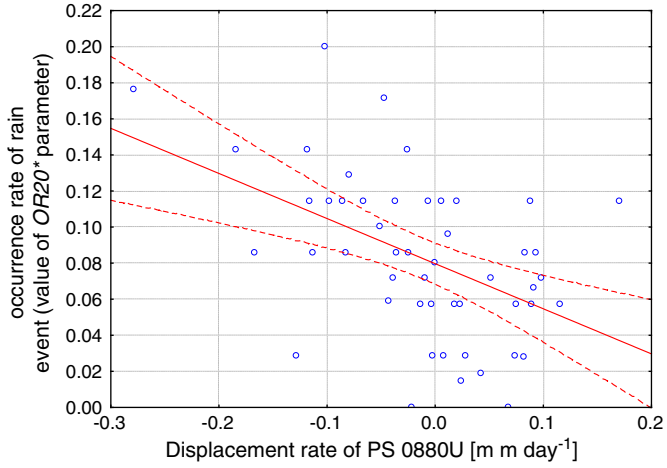

Fig. 4. Scaling of the vertical displacement rate of the permanent scatterer 0880U (Fig. 1) in mm day^{-1} with the occurrence rate of the rainfall event (parameter OR20*). The number of observations is 50, and the correlation is −0.48.

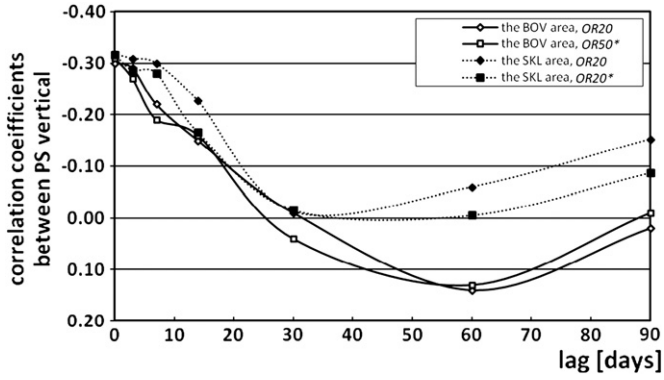

Fig. 6. Correlations between rainfall parameters and permanent scatterer displacement rates, using different time lags for the precipitation dataset. The number of observations is 550 for the BOV area, and 330 for the SKL area.

of −0.40 to −0.76 mm while a rainfall event of intensities higher than ≥20 mm in three successive days results in an elevation change of −1.2 mm (the SKL area). In addition, rain events of ≥50 mm in three successive days were found to result in an average elevation change of −0.87 mm (the BOV area). These elevation changes were sudden or immediate events, as no significant time lag between the rain and elevation change was detected.

Our data also shows that tectonic uplift may play an important role in the soil creep process. Creeping processes could be more active in the areas of more intensive tectonic uplift, provided that geological conditions are also favourable for soil creep. Based on the data from our study, the tectonic uplift in the areas of active soil creep is 13–28 mm year^{-1} larger than the regional tectonic uplift.

Acknowledgements

The authors would like to thank the Research Agency of the Republic of Slovenia (ARRS) for funding this research (grant. no. J1-0913, duration: 1. 2. 2008 to 30. 1. 2011), and the Sedimentology and Mineral Resources programme group (P1-0025) as well as the JTS of Alpine Space–European Territorial Cooperation Programme for co-funding the research through the AdaptAlp project. The authors would also like to

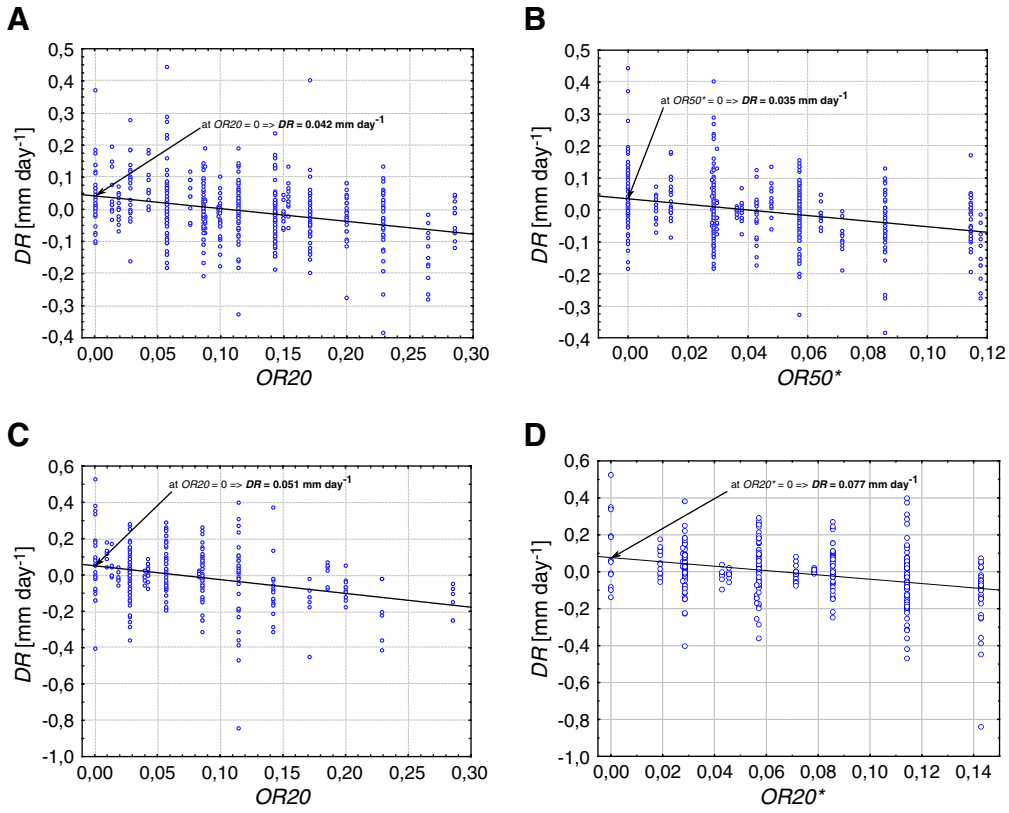

Fig. 5. Scatterplots of the displacement rates of permanent scatterers located in soil creep areas in relation to the intensity of the precipitation. The regression line and the average displacement rate for no precipitation events are indicated. *DR*: displacement rate [mm day^{-1}]. A) 11 permanent scatterers in the BOV area, OR20 precipitation parameter. Regression line: *DR* = 0.042–0.40 OR20; *r* = −0.30; *n* = 550. B) 11 permanent scatterers in the BOV area, OR50* precipitation parameter. *DR* = 0.035–0.87 OR50*; *r* = −0.31; *n* = 550. C) Six permanent scatterers in the SKL area, OR20 precipitation parameter. *DR* = 0.051–0.76 OR20; *r* = −0.32; *n* = 330. D) Six permanent scatterers in the SKL area, OR20* precipitation parameter. *DR* = 0.077–1.2 OR20*; *r* = −0.31; *n* = 330.

Please cite this article as: Žibret, G., et al., PSInSAR displacements related to soil creep and rainfall intensities in the Alpine foreland of western Slovenia, Geomorphology (2012), doi:10.1016/j.geomorph.2012.07.002

thank the reviewers and the editor Takashi Oguchi, for their valuable suggestions and corrections.

References

Ambrosi, C., Crosta, G.B., 2006. Large sackung along major tectonic features in the Central Italian Alps. Engineering Geology 88, 183–200.

ARSO, 2010. Slovenski vremenski rekordi (Slovenian weather records. Last updated on 26 October 2010 Environmental Agency of the Republic of Slovenia, Ljubljana.

Bavec, M., Tulaczyk, S.M., Mahan, S.A., Stock, G.M., 2004. Late Quaternary glaciation of the upper Soča river region (Southern Julian Alps, NW Slovenia). Sedimentary Geology 165, 265–283.

Berardino, P., Fornaro, G., Lanari, R., Sansosti, E., 2002. A new algorithm for surface deformation monitoring based on small baseline differential SAR interferograms. IEEE Transactions on Geoscience and Remote Sensing 40, 2375–2383.

Bovenga, F., Nutricato, R., Refice, A., Wasowski, J., 2006. Application of multi-temporal differential interferometry to slope instability detection in urban/peri-urban areas. Engineering Geology 88, 218–239.

Bovenga, F., Wasowski, J., Nitti, D.O., Nutricato, R., Chiaradia, M.T., 2012. Using COSMO/SkyMed X-band and ENVISAT C-band SAR interferometry for landslides analysis. Remote Sensing of Environment 119, 272–285.

Buser, S., 2010. Geološka karta Slovenije (Geological map of Slovenia. Digital map Geološki zavod Slovenije, Ljubljana.

Calabro, M., Schmidt, D., Roering, J., Douglas, R., 2007. Spatial and temporal characterization of the Portuguese Bend landslide, California, using InSAR. EOS Transactions AGU 88 (52) (Fall Meet. Suppl., Abstract: G53A-07).

Carnec, C., Delacourt, C., 2000. Three years of mining subsidence monitored by SAR interferometry, near Gradane. Journal of Applied Geophysics 43, 43–54.

Colesanti, C., Wasowski, J., 2006. Investigating landslides with space-borne synthetic aperture radar (SAR) interferometry. Engineering Geology 88, 173–199.

Colesanti, C., Ferretti, A., Prati, C., Rocca, F., 2003. Monitoring landslides and tectonic motions with the permanent scatterers technique. Engineering Geology 68, 3–14.

Declerq, P.Y., Devleeschouwer, X., Pouriel, F., 2005. Subsidence revealed by PSInSAR technique in the Ottignies–Wavre area (Belgium) related to water pumping in urban area. In: Lacoste, H., Ouwehand, L. (Eds.), Proceedings of Fringe 2005 Workshop, 28 November–2 December 2005, Frascati, Italy, (ESA SP-610, February 2006). European Space Agency, Noordwijk, Netherlands, pp. 66.1–66.6.

Farina, P., Colombo, D., Fumagalli, A., Marks, F., Moretti, S., 2006. Permanent scatterers for landslide investigations: outcomes from the ESA—SLAM project. Engineering Geology 88, 200–217.

Ferretti, A., Prati, C., Rocca, F., 2001. Permanent scatterers in SAR interferometry. IEEE Transactions on Geoscience and Remote Sensing 39, 8–20.

Ferretti, A., Bianchi, M., Prati, C., Rocca, F., 2005. Higher-order permanent scatterers analysis. EURASIP Journal on Applied Signal Processing 20, 3231–3242.

Fruneau, B., Achace, C., Delacourt, C., 1996. Observation and modelling of the Saint-Etienne-de-Tinee landslide using SAR interferometry. Tectonophysics 265, 181–190.

Guzzetti, F., Cardinali, M., Reichenbach, P., Cipolla, F., Sebastiani, C., Galli, M., Salvati, P., 2004. Landslides triggered by the 23 November 2000 rainfall event in the Imperia Province, Western Liguria, Italy. Engineering Geology 73, 229–245.

Hilley, G.E., Bürgmann, R., Ferretti, A., Novali, F., Rocca, F., 2004. Dynamics of slow-moving landslides from permanent scatterer analysis. Science 304, 1952–1955.

Hinkelmann, R., Zeheb, E., Ehlersc, W., Joswigd, M., 2011. Special section on landslides: setting the scene and outline of contributing studies. Vadose Zone Journal 10, 473–476.

Hu, J.C., Huang, M.H., Tung, H., Ching, K.E., Rau, R.J., Lin, C.W., 2009. Monitoring of active faults in Taiwan by geodetic measurements. In: Koizumi, N., Matsumoto, N., Shieh, C.L. (Eds.), Proceedings of the 7th Japan–Taiwan International Workshop on Hydrological and Geochemical Research for Earthquake Prediction. Geological Survey of Japan. Openfile Report, no. 493.

Iverson, R.M., 2000. Landslide triggering by rain infiltration. Water Resources Research 36, 1897–1910.

Jemec, M., Komac, M., 2011. Rainfall patterns for shallow landsliding in perialpine Slovenia. Natural Hazards 13, http://dx.doi.org/10.1007/s11069-011-9882-9.

Kastelic, V., Vrabec, M., Cunningham, D., Gosar, A., 2008. Neo-Alpine structural evolution and present-day tectonic activity of the eastern Southern Alps: the case of the Ravne Fault, NW Slovenia. Journal of Structural Geology 30, 963–975.

Komac, M., 2006. A landslide susceptibility model using the analytical hierarchy process method and multivariate statistics in perialpine Slovenia. Geomorphology 74, 17–28.

Komac, M., Bavec, M., 2007. Application of PSInSAR for observing the vertical component of the recent surface displacement in Julian Alps. Geologija 50, 97–110.

Komac, M., Ribičič, M., 2006. Landslide susceptibility map of Slovenia at scale 1:250.000. Geologija 49, 295–309.

Lajmiš, L., Žalohar, J., Gregorič, A., Vrabec, M., 2011. Kinematic and paleostress evolution of NW–SE trending "Dinaric" faults in Slovenia — a case for Neogene orogen-perpendicular extension in the External Dinaries. Geophysical Research Abstracts 13 (EGU2011), 12443.

Lollino, G., Arattano, M., Allasia, P., Giordan, D., 2006. Time response of a landslide to meteorological events. Natural Hazards and Earth System Sciences 6, 179–184.

Meisina, C., Zucca, F., Fossati, D., Ceriani, M., Allievi, J., 2006. Ground deformation monitoring by using the permanent scatterers technique: the example of the Oltrepo Pavese (Lombardia, Italy). Engineering Geology 88, 240–259.

Oštir, K., 2000. Analiza vpliva združevanja radarskih interferogramov na natančnost modelov višin in premikov zemeljskega površja (Analysis of joining the interferograms to the precision of elevation models and displacements of earth surface). Ph.D. Thesis, Univ. of Ljubljana, Slovenia.

Oštir, K., 2006. Daljinsko zaznavanje (Remote Sensing). Založba ZRC, Ljubljana.

Oštir, K., Komac, M., 2007. PSInSAR and DInSAR methodology comparison and their applicability in the field of surface deformations — a case of NW Slovenia. Geologija 50, 77–96.

Placer, L., 2008. Osnove tektonske razčlenitve Slovenije (Principles of the tectonic subdivision of Slovenia). Geologija 51, 205–217.

Poljak, M., Živčić, M., Zupančič, P., 2000. The seismotectonic characteristics of Slovenia. Pure and Applied Geophysics 157, 37–55.

Rižnar, I., Koler, B., Bavec, M., 2007. Recentna aktivnost regionalnih geoloških struktur v zahodni Sloveniji (Recent activity of the regional geologic structures in western Slovenia). Geologija 50, 111–120.

Rotaru, A., Oajdea, D., Răileanu, P., 2007. Analysis of the landslide movements. International Journal of Geology 1, 70–79.

Rott, H., Nagler, T., 2006. The contribution of radar interferometry to the assessment of landslide hazards. Advances in Space Research 37, 710–719.

Salvi, S., Atzori, S., Tolomei, C., Allievi, J., Ferretti, A., Rocca, F., Prati, C., Stramondo, S., Feuillet, N., 2004. Inflation rate of the Colli Albani volcanic complex retrieved by the permanent scatterers SAR interferometry technique. Geophysical Research Letters 31, 12606–12610.

TRE, 2008. Analysis of the western Slovenia area with the PS technique™. Tele-Rilevemento Europa, Processing Report Ref: 08.044C (05/06/2008).

Vrhovec, T., Rakovec, J., Gregorič, G., 2004. Mesoscale diagnostics of prefrontal and frontal precipitation in the southeast Alps during MAP IOP 5. Meteorology and Atmospheric Physics 86, 15–29.

Yu, F.C., Chen, T.C., Lin, M.L., Chen, C.Y., Yu, W.H., 2006. Landslides and rainfall characteristics analysis in Taipei City during the Typhoon Nari event. Natural Hazards 37, 153–167.

Zupančič, B., 1995. Klimatografija Slovenije. Količina padavin: obdobje 1961–1990 (Climatic Conditions in Slovenia. Quantity of Rainfall: Between 1961–1990). Environmental Agency of the Republic of Slovenia, Ljubljana.

Please cite this article as: Žibret, G., et al., PSInSAR displacements related to soil creep and rainfall intensities in the Alpine foreland of western Slovenia, Geomorphology (2012), doi:10.1016/j.geomorph.2012.07.002